Nanomaterial with High Antimicrobial Efficacy—Copper/Polyaniline Nanocomposite

Una Bogdanović,[†] Vesna Vodnik,*,[†] Miodrag Mitrić,[†] Suzana Dimitrijević,[‡] Srečo D. Škapin,[§] Vojka Žunič,[§] Milica Budimir,[†] and Milovan Stoiljković[†]

[†]Vinča Institute of Nuclear Sciences, University of Belgrade, P.O. Box 522, 11001 Belgrade, Serbia

[‡]Department of Bioengineering and Biotechnology, Faculty of Technology and Metallurgy, University of Belgrade, Karnegijeva 4, 11000 Belgrade, Serbia

[§]Department of Advanced Materials, Jožef Stefan Institute, Jamova 39, 1000 Ljubljana, Slovenia

Ⓢ Supporting Information

ABSTRACT: This study explores different mechanisms of antimicrobial action by designing hybrid nanomaterials that provide a new approach in the fight against resistant microbes. Here, we present a cheap copper—polyaniline (Cu—PANI) nanocomposite material with enhanced antimicrobial properties, prepared by simple in situ polymerization method, when polymer and metal nanoparticles are produced simultaneously. The copper nanoparticles (CuNPs) are uniformly dispersed in the polymer and have a narrow size distribution (d_{av} = 6 nm). We found that CuNPs and PANI act synergistically against three strains, *Escherichia coli*, *Staphylococcus aureus*, and *Candida albicans*, and resulting nanocomposite exhibits higher antimicrobial activity than any component acting alone. Before using the colony counting method to quantify its time and concentration antimicrobial activity, different techniques (UV—visible spectroscopy, transmission electron microscopy, scanning electron microscope, field emission scanning electron microscopy, X-ray diffraction, Fourier transform infrared spectrophotometry, and inductively coupled plasma optical emission spectrometry) were used to identify the optical, structural, and chemical aspects of the formed Cu—PANI nanocomposite. The antimicrobial activity of this nanocomposite shows that the microbial growth has been fully inhibited; moreover, some of the tested microbes were killed. Atomic force microscopy revealed dramatic changes in morphology of tested cells due to disruption of their cell wall integrity after incubation with Cu—PANI nanocomposite.

KEYWORDS: copper nanoparticles, polyaniline, nanocomposite, antimicrobial activity, AFM
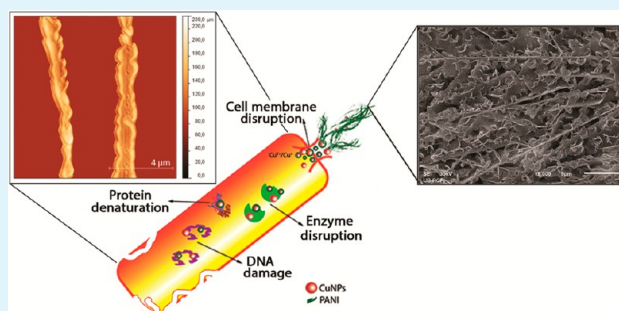
1. INTRODUCTION

As a result of increasing microbial resistance to multiple antimicrobial agents and development of resistant strains, there is an increasing demand for novel antimicrobial materials with superior performance for disinfection applications. In this regard, nanocomposite materials are particularly effective, due to a high surface-to-volume ratio, which provide a large active surface in the contact with microorganisms. Besides, their improved chemical and physical properties different from those of the corresponding bulk materials due to the synergetic combination of two or more components are also important.[1,2] However, development of these materials requires thorough characterization to ascertain their physicochemical properties and to fully understand the mechanisms of their toxicity and safely exploit their antimicrobial properties without negatively impacting human health and the environment.

Commonly used antimicrobial nanocomposite materials include metal ions or NPs (silver,[3,4] copper,[5−7] gold,[8,9] platinum[10]), metal oxide (titanium dioxide,[11] zinc oxide,[7] copper oxide[12]), and organically modified nanoclay.[13] The antimicrobial function of metal ions and NPs has long been recognized and exploited industrially for several purposes, including amendments to textiles and cosmetics, food processing, water treatment, and so on.[14,15] Their antimicrobial activities were inversely proportional to their average size due to a large number of the low-coordinate atoms on the particle surface available to interact with microbial membranes or to release metal ions.[16] The recent interest in the CuNPs is propelled by both the advances of these NPs as a cheap alternative for noble and expensive metal NPs such as gold, silver, and platinum (in the areas of thermal conducting materials and microelectronics applications)[17,18] and the possibility of exploring them as ultimate antimicrobial agent.[5,19−21] Copper toxicity originates not only from the generation of oxidative stress but also from its tendency to alternate between its cuprous, Cu(I), and cupric, Cu(II),

oxidation states, differentiating CuNPs from other metal NPs. Both ion-mediated bactericidal mechanisms involve the inhibition of cellular energy-transducing capabilities and accumulated damage at multiple cellular sites.

Because the CuNPs are very sensitive to air, their advanced applications require appropriate chemical functionalization with organic molecules or their incorporation in suitable polymer matrix, such as conducting polymer PANI, due to its good environmental stability, reversible redox behavior, facile chemistry, low cost, antibacterial properties, and potential in biomedical and other promising applications.[22−24] Several studies suggest that the mechanism of the PANI antimicrobial effect, is a possible reaction of acidic dopants on the polymer chains with the microbes[25] and/or electrostatic attraction between the PANI macromolecules and the microbes.[26] So, in the context of previous reports, it is apparent to prepare Cu−PANI nanocomposite and examine its antimicrobial activity. However, to our knowledge, there are no reports of the antimicrobial activity of Cu−PANI nanocomposite. Hence, ours is the first group to report an antimicrobial activity of as synthesized Cu−PANI nanocomposite against *Escherichia coli*, *Staphylococcus aureus*, and *Candida albicans*, except for the report by Liang et al.[7] in which core−shell CuZnO−PANI nanocomposites exhibit antimicrobial activity against the same strains. The presented results extends our previous work, in which we reported excellent antimicrobial properties of the CuNPs (d_{av} = 5 nm) against the different microorganisms.[27] In this study, we combined distinct and powerful features of both components, CuNPs and PANI, and used atomic force microscopy (AFM) observation to consider morphological changes in microbial cells. Antimicrobial activity was determined using a colony-reduction assay. Furthermore, we performed comparative quantitative tests with PANI alone and clearly demonstrated that synergistic activity of CuNPs and PANI becomes operational when both components act together.

2. EXPERIMENTAL SECTION

2.1. Materials. Copper(II) chloride dihydrate ($CuCl_2 \cdot 2H_2O$) and hydrochloric acid (HCl) were purchased from Sigma-Aldrich and used as received. Aniline monomer (p.a., > 99.5%, Centrohem, Serbia) was distilled under reduced pressure and stored at room temperature, under argon, prior to use. Milli-Q deionized water had an electrical resistivity of 18.2 MΩ and was used as a solvent.

2.2. Synthesis of Cu−PANI Nanocomposite. Cu−PANI nanocomposite was synthesized by a simple process of oxidative polymerization in methanol. For the preparation of this nanocomposite, copper salt ($CuCl_2 \cdot 2H_2O$, 1.2×10^{-1} M) was first dissolved in methanol in a round-bottom flask, and its pH value was adjusted to less than 4 with 1 M HCl. Finally, aniline in molar relation to Cu salt ([aniline]/[$CuCl_2$] = 1/3) was added with stirring. The initial fluorescent green color of copper salt almost immediately turned dark red-brown and then to brownish-green as Cu−PANI nanostructures formed. The mixture was kept under vigorous stirring for 20 h at room temperature. The final solution was first evaporated by rotary evaporator to remove methanol and soluble oligomers. The precipitate was then washed with 5×10^{-3} M HCl and dried at 30 °C. The amount of the Cu in the Cu−PANI nanocomposite determined by ICP-AES was found to be 14.25 wt %. For comparison of antimicrobial activity, pure PANI sample without CuNPs was synthesized using the procedure described in our previous report, where 32.5×10^{-3} M (NH_4)$_2$$S_2$$O_8$ for oxidation of aniline was used instead of $CuCl_2$.[28]

2.3. Characterization Techniques. Ultraviolet−visible (UV−vis) absorption spectrum of the Cu−PANI nanocomposite was acquired by

using a Thermoscientific Evolution 600 spectrophotometer at room temperature. The content of copper in Cu−PANI nanocomposite was determined using an inductively coupled plasma atomic emission spectrometer (ICP-AES) Spectroflame P, operated at 27.12 MHz, 2.5 kW. Before the ICP measurements, the Cu−PANI nanocomposite (10 μL) was dissolved in 5 mL of concentrated nitric acid. To investigate the size and morphological characteristics of the prepared materials, we utilized transmission electron microscopy (TEM). For this purpose, all of the samples were dispersed in methanol and dropped onto carbon-coated copper grid. The analysis of so-prepared samples was performed with a TEM JEOL-JEM-2100, operating at 200 kV. The average particle size and the standard deviation were evaluated on more than 100 particles from different portions of the grid. Selected-area electron diffraction (SAED) was used for crystal structure determination. The morphology and microstructures were analyzed by using a field-emission scanning electron microscope (FE-SEM; Zeiss ULTRA plus) equipped with an energy-dispersive spectrometer (EDXS, Inca 400, Oxford Instruments) and scanning electron microscopy (SEM, JEOL JSM-6610 LV instrument). Fourier transform infrared (FTIR) spectra of the powdered sample was recorded using Thermo Nickolet Corporation Model 380 Fourier Transform IR Spectrophotometer (Attenuated Total Reflection Mode). X-ray diffraction (XRD) patterns were recorded using Bruker D8 Advance diffractometer equipped with focusing Ge-crystal primary mono-chromator (Johanson type) that generates Cu Kα radiation (step time: 6 or 8 s; step: 0.028 deg or 0.058 deg).

2.4. Antimicrobial Assays. The antimicrobial activity of Cu−PANI nanocomposite was assessed against Gram-negative bacteria *E. coli* (ATCC 25922), Gram-positive bacteria *S. aureus* (ATCC 25923), and fungus *C. albicans* (ATCC 10259), using the standard test method ASTM E 2149-01 (ASTM Designation E 2149-01, 2001). Microbial inoculum was prepared in tryptone soy broth (TSB, Torlak, Serbia), supplemented with 0.6% yeast extract (Torlak, Serbia), and left overnight at 37 °C. Then, 9 mL of test sterile physiological saline solutions with different concentrations (1, 2, 5, 10, and 20 ppm) of Cu−PANI was inoculated with 1 mL of inoculum, as was a control sample without nanocomposite. After incubation time of 1 h/2 h at 37 °C, 100 μL aliquots of appropriate dilution were placed in sterile Petri dishes, covered with tryptone soy agar (Torlak, Serbia), and incubated for 24 h at 37 °C. After the incubation period, the colony forming units (CFU) of each plate were determined. Colonies were counted and compared to those on control plates to calculate changes in the cell growth inhibition. The percentage of cell growth reduction (R, %) was calculated using the following equation:

$$R = \frac{C_0 - C}{C_0} \times 100 \tag{2}$$

where C_0 is the number of CFU from the control sample and C is the number of CFU from treated samples. For comparison, antimicrobial activity of PANI without CuNPs was tested by the same method, using the same concentrations as nanocomposite, over 1 and 2 h of incubation time.

2.5. Cell Morphology Study. Microstructure and morphological changes of microbial cells morphology deposited on mica substrate were recorded by Atomic Force Microscopy (AFM) Quesant-Scope Universal Scanning (Ambios Technology, Santa Cruz, CA) and its own software, operating in tapping mode, with the scan rates ranging of 1 Hz. The experiments were done in the same room at room temperature (25 ± 1 °C) and (50 ± 1%) relative humidity. These measurements were performed on microbial cells before and after their contact with the Cu−PANI in the air, using silicon T−shaped cantilevers with a spring constant of 40 N/m on square areas of 1 × 1 μm. All images were obtained at 1 Hz, with a 512 × 512 pixels image definition over different square areas. The images were converted to uncompressed linear 8-bit gray scale TIF format for further analyses and presented in Error image mode and in Broadband (BB) wave mode. The cells were collected from TSB (Tripton soy broth) by centrifugation (13 000 rpm, 1 min) and washed with saline solution two times. Thus, prepared microorganisms were used for incubation

with the Cu−PANI (20 ppm) for 1 and 2 h at 37 °C. After that, cells were fixed for 2 h in 2.5% (v/v) glutaraldehyde (100 mM phosphate buffer solution, pH = 7.0) and washed three times in phosphate buffer (13 000 rpm, 3 min). For AFM analysis, 20 μL of diluted cell suspension was placed on a freshly cleaved mica discs by spin coating technique (3500 rpm for 1 min) and allowed to dry for about 5 min before imaging.

3. RESULTS AND DISCUSSION

3.1. Cu−PANI Nanocomposite Characterization. The formation-growth of CuNPs and PANI was visually monitored by the color change of the methanol fluorescent green solution of the CuCl$_2$ to reddish-brown color immediately after addition of aniline, indicating the formation of the CuNPs and then turned to brownish-green, which is a convincing indication of the formation of PANI. These changes were further confirmed by the absorption spectrum, shown in Figure 1, which contains
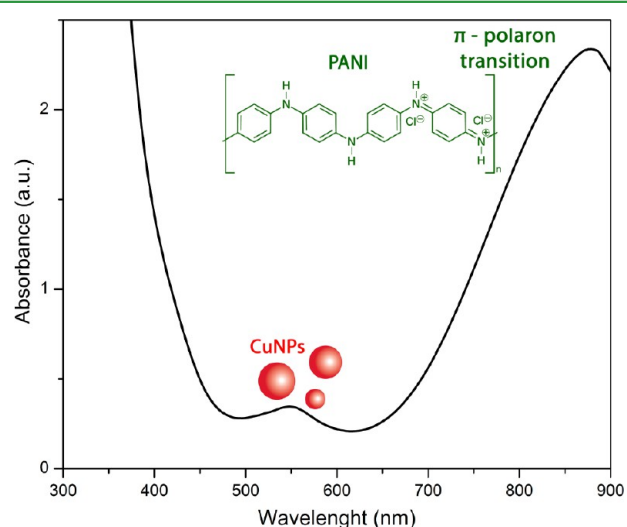

Figure 1. Absorption spectrum of the Cu−PANI nanocomposite.

a surface plasmon resonance (SPR) band of CuNPs at 550 nm due to interband transition of a copper electron from upper level of the valence band and characteristic peak of doped PANI through a protonation by HCl at 880 nm, assigned to π−polaron transition from delocalized free electron states of PANI.[29−32] The second absorption band (880 nm) is moved to a longer wavelength due to the higher doping level of PANI and formation of the long chain polymeric unit, which has been reported previously.[33−36] In addition, interaction between exciton located in the quinoid ring of PANI and surface plasmon of CuNPs is also visible as a blue-shift of the SPR band to 550 nm, comparing with the absorption of CuNPs similar size in the range 560−570 nm, observed in our earlier work.[28]

In addition to the UV−vis measurement, TEM measurement identified that spherical CuNPs with mean diameter of about 6.0 ± 0.2 nm were formed during the polimerization of aniline (Figure 2). They are well separated and dispersed homogeneously throughout the polymer matrix. The detailed structure of the Cu−PANI nanocomposite is further revealed by high-resolution TEM images and an electron diffractogram given in Figure 2c,d. The observed interplanar distance was found to be $d = 0.1974$ nm (Figure 2d), related to the (111) diffraction planes of *fcc* copper structure. The use of electron diffraction (Figure 2c) provides information regarding both the polymer and the CuNPs, and two conclusions can be drawn: (1) the

PANI is semicrystalline, producing the characteristic rings in the diffraction pattern, and (2) the diffraction pattern of CuNPs is in the form of spots superimposed on the rings, which is originated from several different crystallographic orientations. This is a simple manifestation of the crystal shape effect caused by the nanoscale size of the particles and the polycrystalline nature of the NP core.[37] It can be seen that the diffraction pattern in Figure 2c, beside (111) and (200) diffraction planes that belong to Cu, contains (220) plane of CuO, indicating the partial oxidation of CuNPs. The oxidation probably occurred with the particles formed on the surface of the polymer that are not fully protected with polymer molecules. At present, we believe that some fractions of the CuNPs surface are not coordinated to internal PANI branches, which allow their expose to air and facilitate the oxidation.

Further analysis of the morphology and microstructure of the sample by SEM and FESEM showed dendritic nanostructures of Cu−PANI composite with a typical multibranching tree-like form, as seen at low-magnification SEM image in Figure 3a. The individual dendrites have one trunk and branches parallel to each other in the same plane, forming symmetric structures. The length of the trunks is more than a 100 μm, and from the FESEM image (Figure 3c) of a single dendrite structure in much better resolution, the diameter of the side branches is around 25−45 nm. Interestingly, during the growth process of nanocomposite, each branch can also be a trunk to support the growth of PANI. From the FESEM image in Figure 3c, it can be observed that PANI chains are connected to form coral-like dendritic nanofibers. Besides, in these series of images, presented in Figure 3, the important evidence was that nanocomposite dendrites were obtained in a large quantity and good uniformity with pores between the branches nanofibers, since the SEM images at different locations on the sample exhibit similar features. It is important to note that such nanostructures with interconnected conducting matrix and porosities offer greater effective surface areas than bulk materials and could facilitate the transport of electrons and ions.[38] In addition to the morphological analysis, the EDX analysis confirms the presence of Cu along with nitrogen, carbon, oxygen, and chlorine in the Cu−PANI nanocomposite (Figure 3d).

According to results from UV−vis, TEM, and SEM analyses and synthetic route of Cu−PANI nanocomposite shown in the Sheme 1, the formation of branched fibrous PANI is related to both the chemical oxidation polymerization process and the linear nature of the PANI macromolecule chains. Also, the final structure of the nanocomposite depends on the rates of nucleation and growth during the process of the reaction. In this synthesis, the nucleation and growth of CuNPs, and polymerization of aniline takes place simultaneously. For the reduction of CuCl$_2$, the amine nitrogen of aniline acts as sites for reducing the Cu^{2+} ions, while the CuCl$_2$ acts as an oxidizing agent to initiate the polymerization. Thus, the amine units of PANI are transformed to imine units, and CuNPs are formed similar to the reaction of other metal ions with aniline.[32,39,40] During the polymerization, each step involved a release of electrons[41] that in turn reduce the Cu ions to form Cu atoms, which further coalesce to form CuNPs that are encapsulated by the PANI matrix. Because the reduction rate of CuCl$_2$ was fast, the more Cu nuclei were formed during early stage of the reduction, which favored the formation of smaller CuNPs (<10 nm). The PANI formation kinetically controls the growth rates of various faces of CuNPs by selectively adsorbing onto the
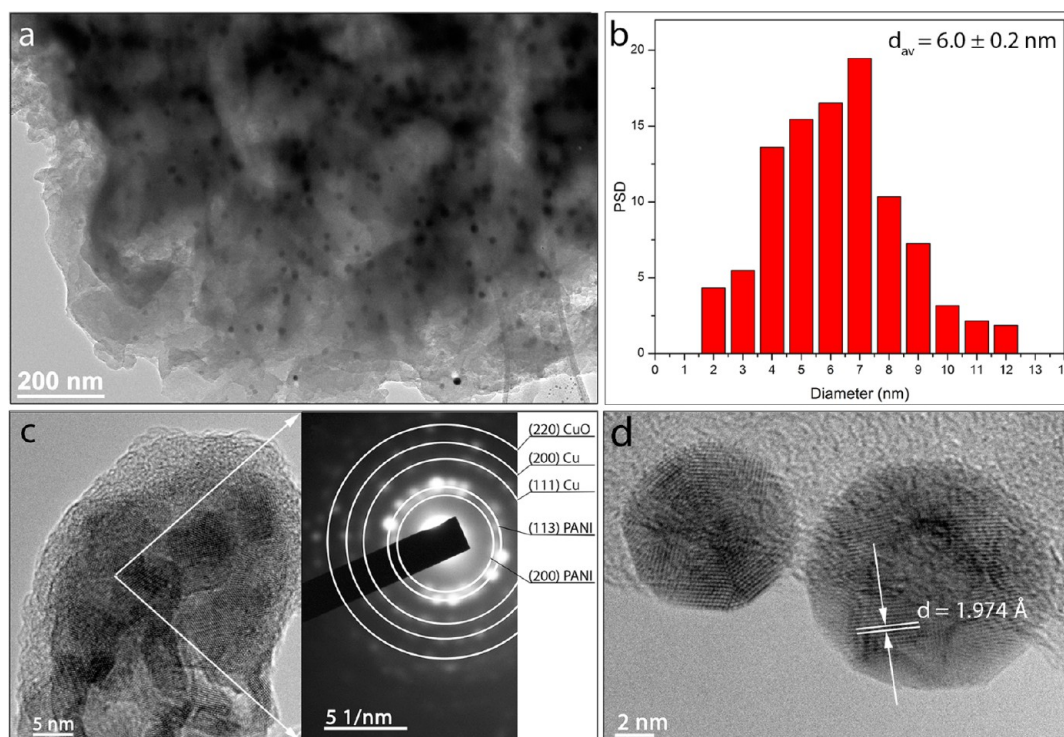
Figure 2. Typical TEM images of the Cu−PANI nanocomposite (a) at low magnification with (b) corresponding particle size distribution (PSD); (c) high-magnification view of an individual Cu−PANI branche with selected area electron diffraction (SAED) patterns; and (d) HRTEM image with fringe spacing.
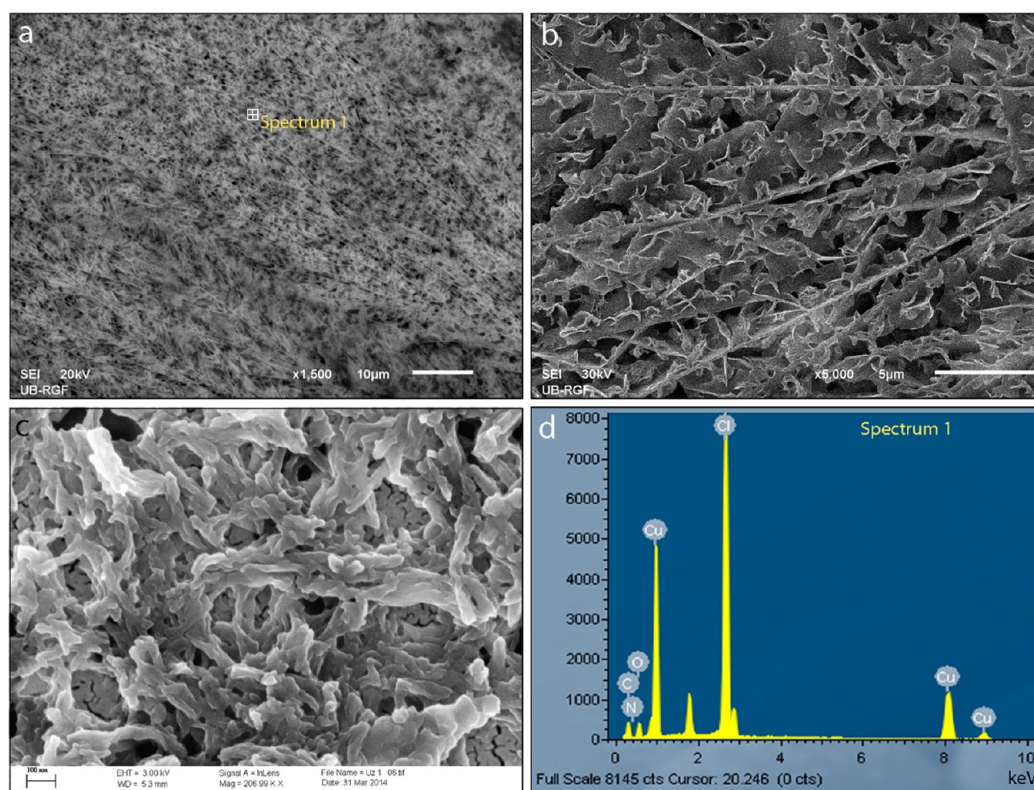

Figure 3. (a) Low- and (b) high-magnification SEM images of dendritic Cu−PANI nanocomposite; (c) FESEM image; (d) EDX spectrum obtained from the image (a).

crystallographic planes, which was previously discussed. In addition, the formation of oxidized polymer-emeraldine salt (as we showed from the UV−vis analysis) with delocalized positive charges, provided both steric and electrostatic stabilization, protecting the CuNPs as stable colloidal forms. On the other hand, CuNPs served as the nucleation center for the growth of
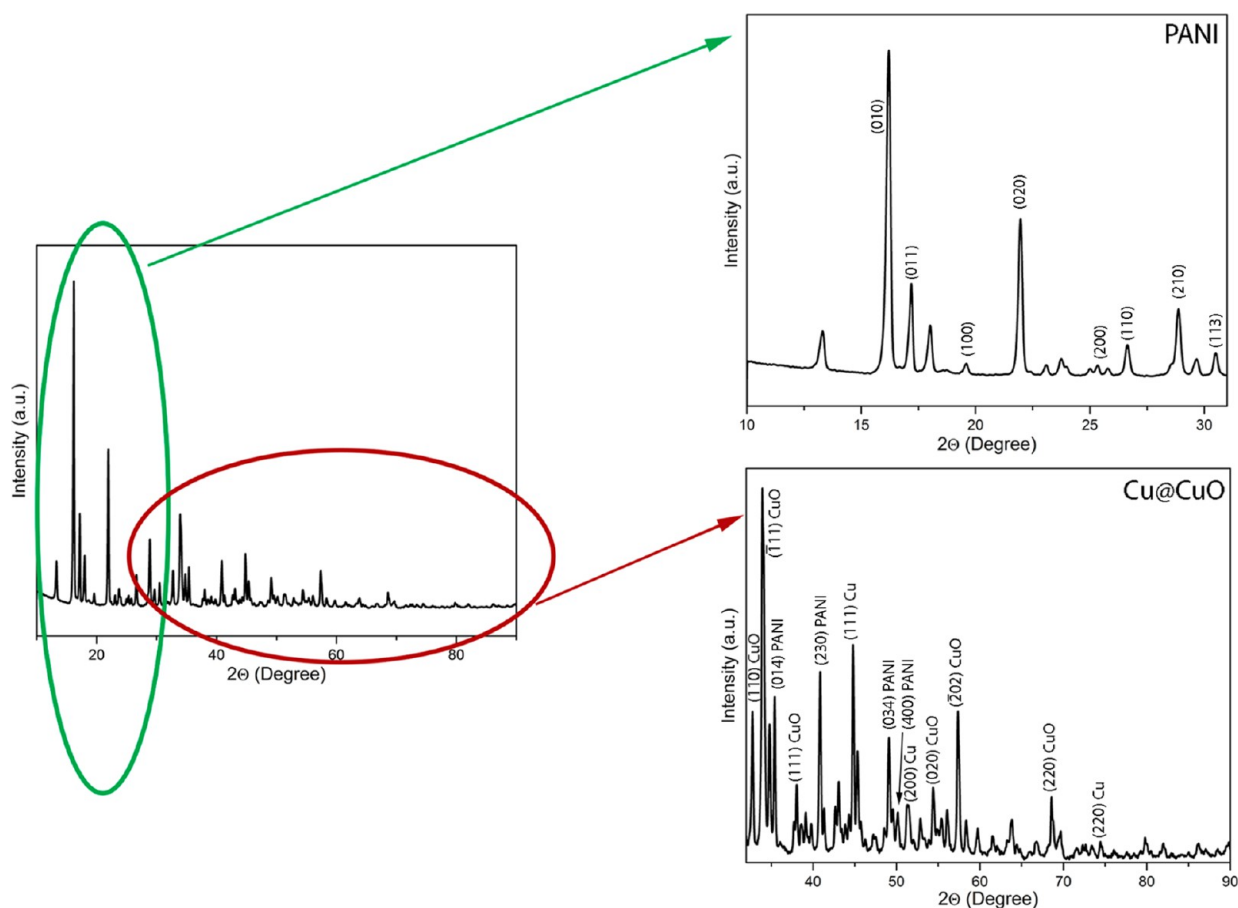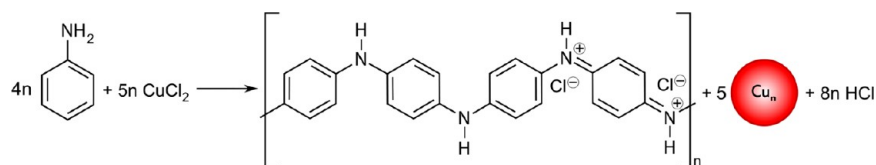
Scheme 1. Synthesis of Cu−PANI Nanocomposite

Figure 4. XRD pattern of Cu−PANI nanocomposite powder.

PANI nanofibers and effectively catalyzed the oriented growth of the polymer, which results in a dendritic morphology. It is important to note that formed π-conjugated PANI has strong electrondonating properties, and could also reduce Cu ions via the electron transfer to the Cu ions, leading to the formation of CuNPs.

The detailed structure of the dendritic Cu−PANI nanocomposites is further revealed by XRD analysis. The XRD pattern shows that the PANI is partly crystalline (Figure 4) with strongest diffraction peaks centered at $2\theta \sim$ 13.3, 16.0, 17.2, 18.0, 19.6, 21.9, 26.6, 28.9, and 30.5°. The peaks at ~16.0, 19.6, and 26.6° have been ascribed to (010), (100), and (110) reflections of polymer in emeraldine salt form.[42,43] Similar to the PANI prepared by conventional methods,[30,44,45] the peaks at 19.6 and 26.6° arise from the periodicity parallel and perpendicular to the polymer chains of PANI, respectively.[45] Additional peaks in the XRD pattern of PANI are also observed at $2\theta \sim$ 38.9, 41.1, 48.5, and 50.0°.[42] In comparison with previous reports of metal−PANI nanocomposites,[29,46] synthesized Cu−PANI nanocomposite show better organized crystalline structure of PANI chains. Because the PANI structure varies from amorphous to partially crystalline depending on the polymer doping state,[45] these results suggest the formation of highly conducting emeraldine salt form of PANI in the samples. On the other hand, the XRD pattern (Figure 4) shows that the synthesized NPs are crystallized in polycrystalline form. It consists of sharp peaks at $2\theta \sim$ 44.8, 51.2, and 74.1°, which correspond to diffraction from the (111), (200), and (220) planes of copper metal, respectively, crystallized in cubic space group $Fm\bar{3}m$, No. 225 (PDF2 89-2838). In addition to the peaks from the pure copper, there are more peaks corresponding to the CuO, crystallized in the monoclinic space group ($C2/c$), No. 15 (PDF2 89-2529), as shown in Figure 4. This result confirms that the synthesized nanoparticles get oxidized with time and the CuNPs converted into Cu@CuO. The oxidation of CuNPs probably ensues after their aging because these small CuNPs are highly reactive due to increased surface area. The presence of copper oxides on the surface of nanoparticles is desirable from the standpoint of antimicrobial application, which will be further discussed at a later point in the paper.

The molecular structure of prepared Cu−PANI nano-composite characterized by FTIR spectroscopy is shown in Figure 5. The presence of PANI is confirmed by the
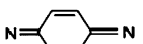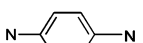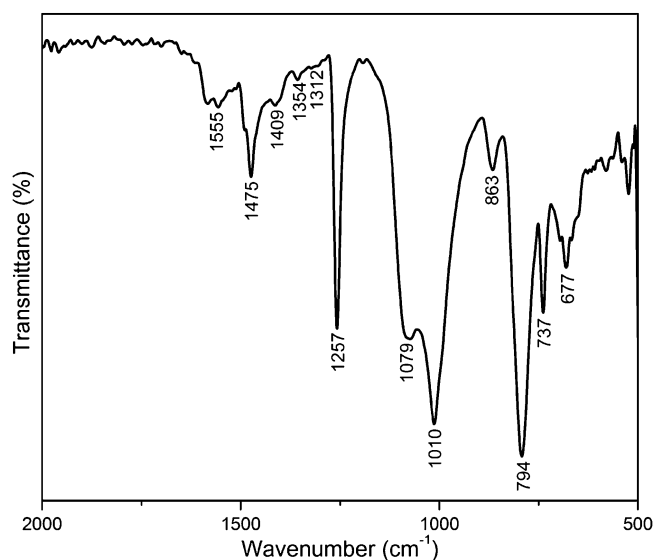

Figure 5. FTIR spectrum of the Cu−PANI nanocomposite.

characteristic peaks in its oxidized emeraldine salt form at the fingerprint region (600−1700 cm^{-1}), with band assignments given in Table 1. The FTIR result indicates that the structure of

Table 1. Characteristic Vibration Modes in the FTIR Spectrum of Cu−PANI Powder

Wavenumber (cm^{-1})	Assignment
1555	quinonoid (Q) ring stretching[48]
1475	benzenoid (B) ring stretching[48]
1409	ring stretching of Phenazine − type segments[28]
1354	C-N stretching vibrations of aromatic amines[51]
1312	C-N stretching vibrations of secondary aromatic amine[51]
1257	C-N$^{+•}$ stretching vibrations in polaron form of PANI emeraldin salt[51]
1079 1010	N-H stretching vibrations in the charged polymer units[28]
863 794 737 677	C-H out-of-plane deformation vibrations of 1,4 − disubstituted benzene ring[28]

the polyaniline backbone in Cu−PANI nanocomposites is similar to that of conventional HCl doped PANI synthesized by a well-established method.[47] The characteristic bands for well-doped PANI salt at 1555 cm^{-1} assigned to C═C quinonoid (Q) ring stretching, and at 1475 cm^{-1} assigned to C═C benzenoid (B) ring stretching,[48] appear at lower wavenumbers than those for the hydrochloric acid doped PANI obtained in the previous report[47] (the bands appeared at 1579 and 1493 cm^{-1}). The shift of these bands can be rationalized as occurring

due to the change in the electron density near the B and Q units of PANI in the presence of the CuNPs, similar to the reports working with Au[28] and CuO nanoparticles.[49] The band at 1354 cm^{-1} is also shifted to lower energy, indicating that amino and imino bonds within the polymer are influenced by the CuNPs.[50] Furthermore, it was observed the presence of phenizene (Phz)-type segments in the PANI as a weak band at 1409 cm^{-1}; these segments formed due to the oxidative intramolecular cyclization of branched oligoaniline and PANI chains.[28] The appearance of the intense broad band consisting of two bands at 1010 and 1079 cm^{-1} can be attributed to N−H stretching vibrations in charged polymer units B−NH$^+$=Q and/or B−NH$^{+•}$−B.[28] The IR analysis implies that the electron density of the C−N bond is perturbed by the presence of the CuNPs in the PANI matrix.

3.2. Evaluation of Cu−PANI Antimicrobial Activity. The antimicrobial efficiency of the Cu−PANI nanocomposite of different concentration was tested against representative microorganisms of public interest (*E. coli*, *S. aureus*, and *C. albicans*), which are widely applied as biological indicators of pollution and contamination in water and hospital instruments. The time and concentration of antimicrobial activity were quantified by the colony counting method, and the results of the biological activity trials over 1 and 2 h incubation time are summarized in Tables S1−S3 (Supporting Information). Figure 6 illustrates the reduction ability of Cu−PANI from the data in
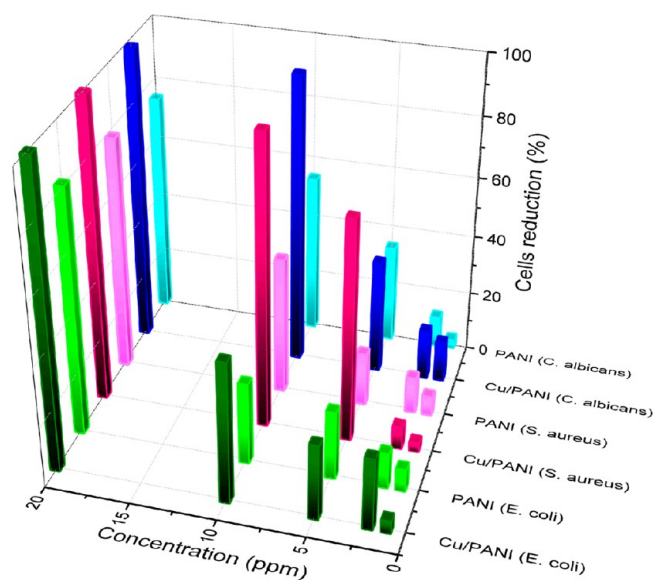

Figure 6. Concentration-dependent reduction ability of the Cu−PANI and PANI on (green) *E. coli*, (pink) *S. aureus*, and (blue) *C. albicans* over 1 h of incubation time.

the Tables over 1 h of incubation time in relation to the concentration of used nanocomposite. A comparably striking antimicrobial activity was also exerted on the pristine PANI, and the results are reported in the Tables S1−S3 (Supporting Information) and Figure 6.

Various concentrations of the CuNPs required for growth inhibition or killing the strains were influenced by the biological properties of individual species. To minimize the nanocomposite toxicity toward untargeted cells, its low concentrations were chosen (≤20 ppm). The obtained results show that higher nanocomposite or pristine PANI concentrations have a corresponding lower number of CFUs, that is, a stronger
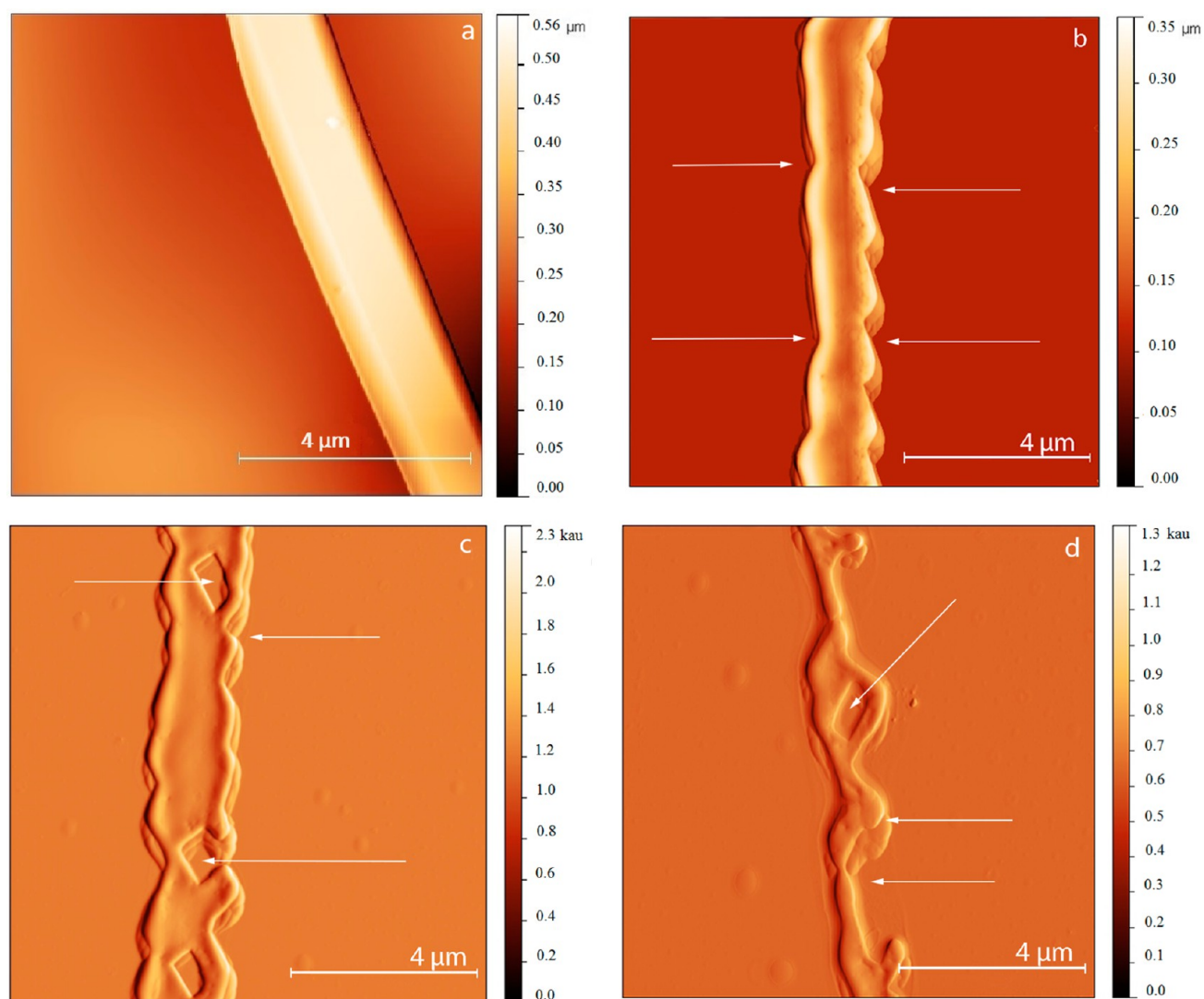
Figure 7. AFM images of *E. coli* (a) before and after incubation with Cu−PANI nanocomposite (20 ppm) for (b) 1 h and (c and d) 2 h. The images are presented in (a and b) BB wave mode and in (c and d) Error mode.

antimicrobial effect. After 1 h, CFUs were reduced significantly with increasing the Cu−PANI concentration in the growth medium. At this time, the almost complete growth inhibition was achieved (99.9% microbial reduction) against *E. coli* and *S. aureus* and slightly smaller fungal reduction (97.9%) with the Cu−PANI at highest concentration of 20 ppm. On the other hand, over the 1 h exposure time, the pristine PANI was able to reduce ≤81.5% of all tested strains at all PANI concentration. The results also indicate that *E. coli* bacteria is very sensitive toward the nanocomposite, while the least sensitive were the fungus *C. albicans*. Furthermore, the data given in Tables S1−S3 (Supporting Information), clearly demonstrate that no microbial growth was found over the 2 h exposure time for all test concentrations of Cu−PANI nanocomposite (1, 2, 5, 10, and 20 ppm). This means that it took only 2 h for Cu−PANI to completely inhibit the growth of bacteria and fungus and to reach the maximum decrease, as compared to the control in the number of microbial colonies (<10), when the nanocomposite concentration was 1 ppm or higher. This result showed remarkable and very fast antimicrobial activity of nanocomposite in contact with selected microorganisms. It is clear from the above results that Cu−PANI nanocomposite has

better activity when compared to the pristine polyaniline (Figure 6). Moreover, this efficacy is higher over 1 h of incubation time at the lower nanocomposite concentration (1, 2, 5 ppm) than activity of individual CuNPs over 2 h of incubation time at the slightly higher concentration (8, 16, and 32 ppm), obtained in our previous report.[27] At the same time, the growth inhibition of all tested strains in the presence of pristine PANI is smaller than in the presence of previously reported CuNPs. Comparing the results of antimicrobial activity of individual CuNPs,[27] PANI alone, and Cu−PANI nanocomposite, it can be seen that the activity of nanocomposite is more pronounced, than activity of any component acting alone. The results indicated that a synergistic activity of CuNPs and PANI becomes operational, that is, the effectiveness of this action becomes higher when both components act together. In addition, our results suggest that the antimicrobial property of Cu−PANI is effective faster at a much lower concentration than those used for other nanocomposites.[7,8,52] Using the disc diffusion method, which cannot be directly correlated with our test procedure, Boomi et al. shown an antibacterial activity toward 25−150 μg/mL polyaniline−Au-Pd nanocomposite (incubation time is 24 h)[8]
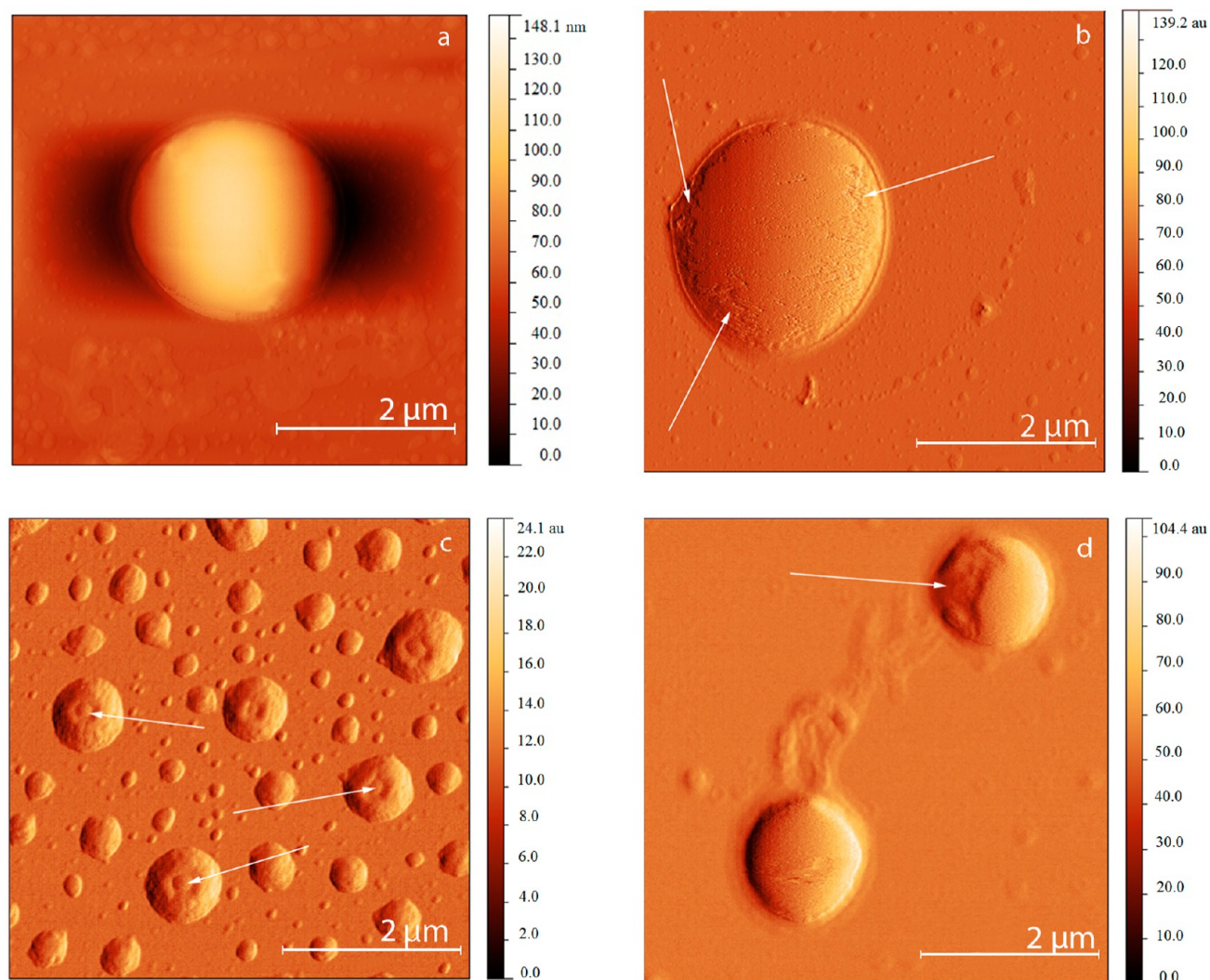
Figure 8. AFM images of *S. aureus* (a) before and after incubation with Cu−PANI nanocomposite (20 ppm) for (b) 1 h and (c and d) 2 h. The images are presented in (a) BB wave mode and (b−d) in Error mode.

and toward 100 μg/mL PANI−Ag-Au nanocomposite (incubation time is 48 h) in the second report.[52] Liang et al. demonstrated that PANI/CuZnO nanocomposite (incubation time is 24 h) show excellent bacteriostatic and bactericidal activities against *E. coli*, *S. aureus*, and *C. albicans* at the concentration of 10−80 μg/mL.[7]

3.3. Effects of Nanocomposite on Cellular Morphology Using AFM. To improve the above observation, we designed further experiments to follow the possible changes in the morphology of treated strains. For this purpose, the AFM measurements were performed before and after 1 and 2 h of their exposed to Cu−PANI nanocomposite (20 ppm).

The AFM analysis of untreated *E. coli* shows isolated rod-shaped cells a relatively smooth surface with compact and intact cell wall (Figure 7a). After 1 h of incubation with Cu−PANI nanocomposite, the cells loss their membrane integrity (Figure 7b) with many indentations on the cell wall (indicated by arrows). The visible rupture of highly sensitive inner membrane, can initiate leakage of essential solutes, which in turn, can have a desiccating effect. The most dramatic changes in the cell wall were observed when the cells were exposed to the nanocomposite for 2 h (Figure 7c,d): the bacteria cell was damaged severely, the cell membrane collapsed, and large pits/

cavities formed along the inside of *E. coli* cells, in the center of the cell (indicated by arrows). The width and length of the hole were found to be 0.6 and 1.1 μm, respectively. This implies that cells are killed and suggests that Cu−PANI-bacterial cell interaction is very strong. From these data, we can envision that the susceptible strain formed additional grooves when the incubation time was extended to 2 h. At this stage, no surviving *E. coli* cells were found. The result indicated that the killing of *E. coli* cells is due to direct damage to the cytoplasmic membrane. The wall mechanical strength of Gram-negative bacteria is provided by a thin peptidoglycan layer (7−8 nm) consisting of glycan chains of alternating *N*-acetylglucosamine and *N*-acetylmuramic acid residues, which are cross-linked by short peptide chains. This layer is overlaid by an outer membrane, a bilaminar structure composed of tightly packed phospholipids and lipopolysaccharides containing membrane proteins (e.g., porins), which increase the negative charge of the cell membrane.[53,54] The observed damages indicated that the electrostatic interaction between the Cu−PANI and membrane anionic phospholipids reside, causing direct damage to the cytoplasmic membrane, thereby compromising the integrity of the cells and leading to bacterial cell death.[55]
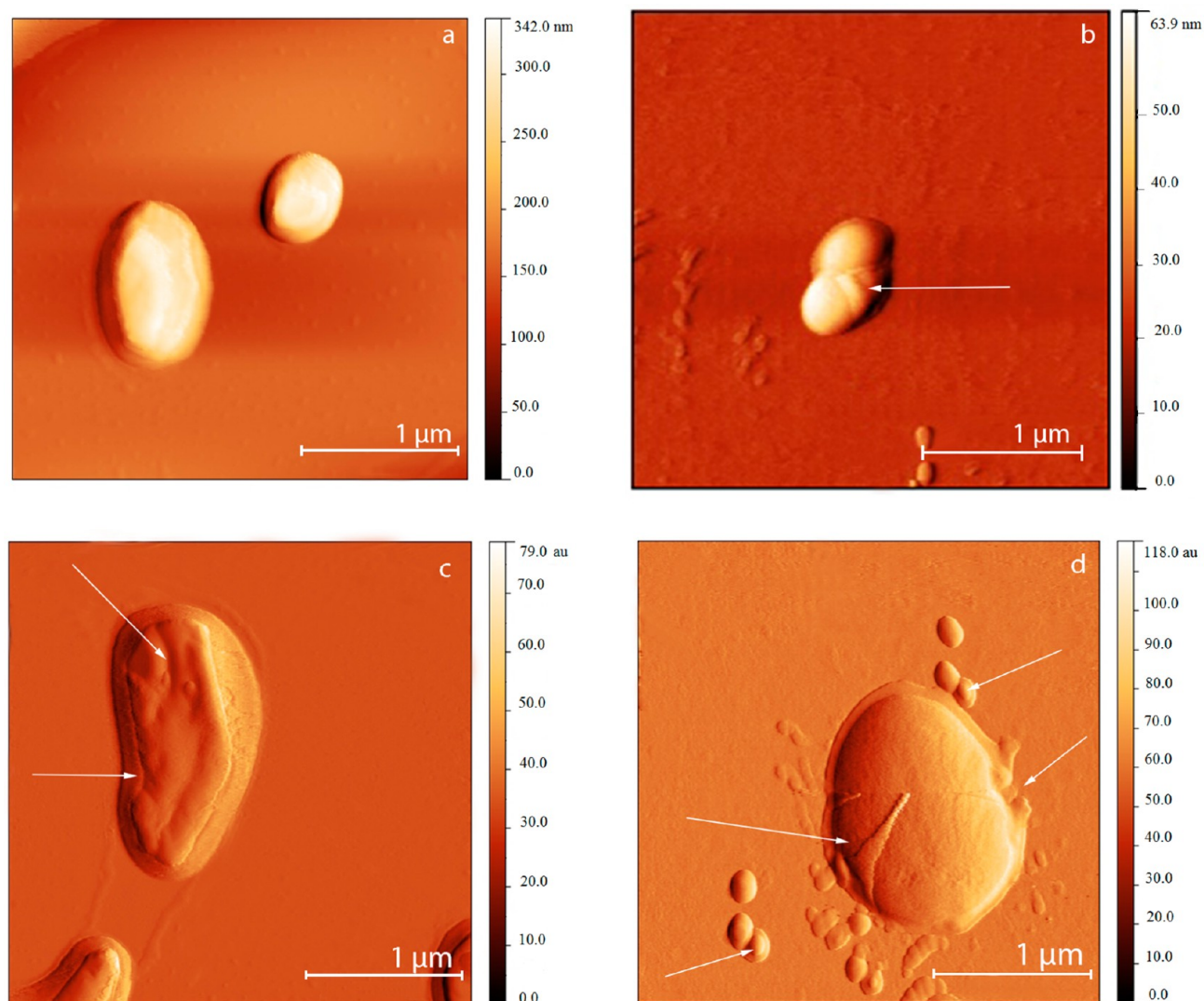
Figure 9. AFM images of (a) untreated *C. albicans* cells and treated cells after incubation with Cu−PANI nanocomposite (20 ppm) for (b) 1 h and (c and d) 2 h. The images are presented in (a and b) BB wave mode and (c and d) Error mode.

The effect of the Cu-PANI on *S. aureus* was found to be quite different from that on *E. coli* cells, although the concentration of the Cu-PANI was the same for these two tested strains. As shown in Figure 8a, the typical near-spherical shape cocci existed as individual cell. After 1 h of treatment, cell surface appeared to be damaged (indicated by arrows, Figure 8b), with a greatly roughened surface texture compared to the smooth surfaces of the untreated cell. In this case, the cell membrane was not collapsed and most of intracellular components were still kept in the bacteria cell, so bacteria were still alive. When the treated time was extended to 2 h, the cells with roughened surface texture and a shallow grooves were found at the midpoint of a cell, indicated by arrows in Figure 8c. In this stage, the cells with leaked inner contents were also found (Figure 8d). The cell walls of Gram-positive bacteria are composed of a complex three-dimensional peptidoglycan network along with covalently bound carbohydrates and cell wall associated proteins.[56,57] Also, the peptidoglycan layer is bound to anionic polymers (e.g., teichoic acid), and it is a thick layer (20−80 nm), which provides an additional protective barrier to harmful elements in the environment. In a three-dimensional peptidoglycan network, peptide portion of the glycan strand can participate in the Cu uptake process[58] especially amine and carboxyl groups of this layer. Also, deposition of the released Cu (II) ions in the cell wall occurs through these groups, which may be the result of the cell wall damages.

The AFM images of the *C. albicans* untreated and treated cells (Figure 9), also revealed considerable morphological alterations in the *C. albicans* induced by the presence of the Cu−PANI nanocomposite. Untreated cells have well-defined, intact shapes with smooth surfaces (Figure 9a). After nanocomposite treatment for 1 h, the membranes of *C. albicans* was perforated, and their shapes became irregular and appeared shrunken compared to the untreated cells (Figure 9b). The cells treated 2 h with the Cu−PANI were further shrunken and their surfaces were wrinkled, as shown in Figure 9c. In both cases, the surface roughness increased as the treatment time increased. However, in the 2 h image, smaller *C. albicans* cells showed several differences from the bigger ones. Cracks were observed on the cell wall, and some of the cells show defective budding (Figure 9d, arrows). In yeast, the cellular wall is composed of the outer layers, enriched for mannoproteins (highly glycosylated polypeptides), and the inner layer,

enriched for chitin, a linear polysaccharide of β1−4 linked *N*-acetylglucosamine, and microfibrillar array of β1−3 glucan overlaid by β1−6 glucan, which create a polysaccharide matrix associated with structural rigidity.[59,60] Chitin is concentrated (90%) in the cell wall, septa, and bud scars, and its defect leads to lysis of the yeast cell.[61] Because the chitin synthesis is regulated by ergosterol, the defective budding observed on the smaller cells can be explained by a disruption of the dynamic relationship between ergosterol and chitin synthesis. The presence of a rigid cell wall and its hydrophobic components play a key role in preventing the Cu-PANI to create more damage to the cell wall, only to disrupt its potential.

According to the previous experiments, we demonstrated that the susceptibility of *E. coli* to Cu−PANI is significantly higher in comparison to *S. aureus* and *C. albicans*. This was somewhat expected because the *S. aureus* is constituted by substantially thicker peptidoglycan layer (lacking the outer membrane) which prevents the penetration of NPs inside the cytoplasm, than the *E. coli* bacteria with a thin peptidoglycan layer and outer membrane. Furthermore, these cells (*S. aureus* and *C. albicans*) produce antioxidative enzyme−catalase and additional alkyl hydroperoxide reductase and staphyloxanthin, which complement catalase to protect them from oxidative damage.[62] This enzyme increase their resistance against Cu−PANI compared to *E. coli*. On the other hand, the difference in cell wall composition of *E. coli* compared to *S. aureus* and *C. albicans* explains its low resistance against Cu−PANI.

The above results provide evidence that the synergistic effect of both components, polymer matrix−PANI and CuNPs, plays a vital role in determining antimicrobial efficacy of the nanocomposite as compared to the individual components. The PANI component showed antibacterial efficacy due to the protonation of nitrogen-containing groups of the long-chain polymer[7,23] and due to the length and morphology of the polymer chain, which contribute to direct physical interaction between the microbial cell and the composite. The dendritic morphology of PANI with interconnected nanofibers offers a greater surface area in direct physical interaction between them. This structure more easily covers cells that cannot proliferate once fully covered, resulting in the cell viability loss observed in the subsequent colony counting test. Also, PANI could prevent the nutrient-uptake process of the microbes from the surroundings, allowing to increase the interaction between CuNPs and the microbes. On the other hand, copper, both as a NPs and in ionic form, exhibits strong cytotoxicity toward a broad range of microorganisms, and its toxicity is largely due to redox cycling reactions that occur at the surface of the cells between Cu^{2+}/Cu^+ ions,[63] which act as electron donor and electron acceptor and have a high impact in electron transport chain and oxygen transportation.[64] The formation reactive oxygen species (ROS) in the contact with CuNPs is probably due to exchange interactions between the electrons from the conduction band of CuNPs and unpaired electrons of the free radicals, similar to gold nanoparticles reported earlier.[65] Similar to previous studies in which oxidized CuNPs enhanced antibacterial activity compared to elemental Cu[20,66] due to the release of Cu^{2+} ions in solution,[67] partial oxidation of our CuNPs in the nanocomposite could enhance antimicrobial activity of the nanocomposite. It is important to note that the microbial properties of such NPs are size-dependent, and the only NPs that present a direct interaction with the microbes preferentially have a diameter of ~1−10 nm.[68] Therefore, the size of the formed CuNPs in the Cu−PANI nanocomposite

could be another factor of its pronounced antimicrobial activity. In addition, as the reactivity of nanoparticles is favored by high atom density facets such as (111),[68,69] the high reactivity of the CuNPs formed in the present nanocomposite, that contain (111) facet is expected.

From the above observation, the synergistic effect of both components might be explained by the combination of the different mechanisms of action of the PANI and CuNPs components: (1) physical interaction and electrostatic contact play a vital role in determining antimicrobial efficacy of the nanocomposite; (2) PANI leads to steric stabilization and decreased aggregation potential of CuNPs, which in turn increases the effective concentration of CuNPs capable of interacting with the cellular surface; (3) PANI nanofibers network increases the interface area between the nanocomposite and microbes, allowing CuNPs to interact with the surface groups of cell walls; (4) the slow oxidation of CuNPs resulting into release of Cu^{2+} ions from the CuO layer and their partially reduction to the Cu^+ ions, which are energetically easier to move across a lipid bilayer and taken up by the cell, causing its damage.

4. CONCLUSIONS

The primary significance of this study is the observation that Cu−PANI nanocomposite can inhibit the growth and kill microbes by acting on a common target—the cell membrane. The study is also significant because the facile synthesis method of Cu−PANI nanocomposite described here is cost-effective. Also, our results suggest that the antmicrobial property of Cu-PANI is effective faster at a much lower concentration than those used for other nanocomposites. It should be noted that such a low nanocomposite concentration over a 2 h exposure time with microbes was enough to reach high antimicrobial efficacy. High population density of CuNPs in the PANI matrix, their small size and spherical shape with highly reactive facets (111), and the large surface area of interconnected conducting polymer nanofibers in the dendritic structure of the Cu−PANI nanocomposite may significantly contribute to the improved antimicrobial activity. AFM imaging provided evidence of a direct and strong interaction between the nanocomposite and the cell wall, leading to the destruction of the cell wall. The results suggest that prepared Cu−PANI nanocomposite may serve as a template for the development of novel antibacterial and antifungal agent. Therefore, we anticipate that Cu−PANI nanocomposite would be an ideal platform for controlling microbial infections and water disinfection applications. Finally, the presented Cu−PANI nanocomposite is also an attractive feature for high-performance chemical and biological sensing, which provides an interesting focus for our future works.

■ ASSOCIATED CONTENT

Ⓢ Supporting Information

Time and concentration antimicrobial activity of Cu/PANI nanocomposite and pure PANI quantified by the colony counting method. This material is available free of charge via the Internet at http://pubs.acs.org.

■ AUTHOR INFORMATION

Corresponding Author

*E-mail: vodves@vinca.rs. Tel: +381113408428. Fax: +381113408607.

■ **REFERENCES**

(1) Holtz, J. H.; Asher, S. A. Polymerized Colloidal Crystal Hydrogel Films as Intelligent Chemical Sensing Materials. *Nature* **1997**, *389*, 829−832.

(2) Willner, I.; Willner, B.; Katz, E. Biomolecule−Nanoparticle Hybrid Systems for Bioelectronic Applications. *Bioelectrochemistry* **2007**, *70*, 2−11.

(3) Tamboli, M. S.; Kulkarni, M. V.; Patil, R. H.; Gade, W. N.; Navale, S. C.; Kale, B. B. Nanowires of Silver−Polyaniline Nanocomposite Synthesized via in Situ Polymerization and Its Novel Functionality as an Antibacterial Agent. *Colloid. Surf. B* **2012**, *92*, 35−41.

(4) Vukoje, I. D.; Džunuzović, E. S.; Vodnik, V. V.; Dimitrijević, S.; Ahrenkiel, S. P.; Nedeljković, J. M. Synthesis, Characterization and Antimicrobial Activity of Poly(GMA-co-EGDMA) Polymer Decorated with Silver Nanoparticles. *J. Mater. Sci.* **2014**, *49*, 6838−6844.

(5) Cioffi, N.; Torsi, L.; Ditaranto, N.; Tantillo, G.; Ghibelli, L.; Sabbatini, L.; Bleve-Zacheo, T.; D'Alessio, M.; Zambonin, P. G.; Traversa, E. Copper Nanoparticle/Polymer Composites with Antifungal and Bacteriostatic Properties. *Chem. Mater.* **2005**, *17*, 5255−5262.

(6) Cady, N. C.; Behnke, J. L.; Strickland, A. D. Copper-based Nanostructured Coatings on Natural Cellulose: Nanocomposites Exhibiting Rapid and Efficient Inhibition of a Multi-drug Resistant Wound Pathogen, *A. baumannii*, and Mammalian Cell Biocompatibility in Vitro. *Adv. Funct. Mater.* **2011**, *21*, 2506−2514.

(7) Liang, X.; Sun, M.; Li, L.; Qiao, R.; Chen, K.; Xiao, Q.; Xu, F. Preparation and Antibacterial Activities of Polyaniline/$Cu_{0.05}Zn_{0.95}O$ Nanocomposites. *Dalton. Trans.* **2012**, *41*, 2804−2811.

(8) Boomi, P.; Prabu, H. G. Synthesis, Characterization, and Antibacterial Analysis of Polyaniline/Au−Pd Nanocomposite. *Colloid Surface A* **2013**, *429*, 51−59.

(9) Mei, L.; Zhang, X.; Wang, Y.; Zhang, W.; Lu, Z.; Luo, Y.; Zhao, Y.; Li, C. Multivalent Polymer−Au Nanocomposites with Cationic Surfaces Displaying Enhanced Antimicrobial Activity. *Polym. Chem.* **2014**, *5*, 3038−3044.

(10) Ma, S.; Izuta, N.; Imazato, S.; Chen, J.-H.; Kiba, W.; Yoshikawa, R.; Takeda, K.; Kitagawa, H.; Ebisu, S. Assessment of Bactericidal Effects of Quaternary Ammonium-based Antibacterial Monomers in Combination with Colloidal Platinum Nanoparticles. *Dent. Mater. J.* **2012**, *31*, 150−156.

(11) Zhang, H.; Chen, G. Potent Antibacterial Activities of Ag/TiO_2 Nanocomposite Powders Synthesized by a One-Pot Sol−Gel Method. *Environ. Sci. Technol.* **2009**, *43*, 2905−2910.

(12) Ojas, M.; Bhagat, M.; Gopalakrishnan, C.; Arunachalam, K. D. Ultrafine Dispersed CuO Nanoparticles and their Antibacterial Activity. *J. Exp. Nanosci.* **2008**, *3*, 185−193.

(13) Rhim, J. W.; Hong, S.-I.; Park, H.-M.; Ng, P. K. W. Preparation and Characterization of Chitosan-based Nanocomposite Films with Antimicrobial Activity. *J. Agric. Food Chem.* **2006**, *54*, 5814−5822.

(14) Mueller, N. C.; Nowack, B. Exposure Modeling of Engineered Nanoparticles in the Environment. *Environ. Sci. Technol.* **2008**, *41*, 4447−4453.

(15) Ilić, V.; Šaponjić, Z.; Vodnik, V.; Potkonjak, B.; Jovančić, P.; Nedeljković, J.; Radetić, M. The Influence of Silver Content on Antimicrobial Activity and Color of Cotton Fabrics Functionalized with Ag Nanoparticles. *Carbohyd. Polym.* **2009**, *78*, 564−569.

(16) Carlson, C.; Hussain, S. M.; Schrand, A. M.; Braydich-Stolle, L. H.; Hess, K. L.; Jones, R. L.; Schlager, J. J. Unique Cellular Interaction of Silver Nanoparticles: Size-Dependent Generation of Reactive Oxygen Species. *J. Phys. Chem. B* **2008**, *112*, 13608−13619.

(17) Eastman, J. A.; Choi, S. U. S.; Li, S.; Yu, W.; Thompson, L. Anomalously Increased Effective Thermal Conductivities of Ethylene Glycol Based Nanofluids Containing Copper Nanoparticles. *J. Appl. Phys. Lett.* **2001**, *78*, 718−720.

(18) Lu, L.; Sui, M. L.; Lu, K. Cold Rolling of Bulk Nanocrystalline Copper. *Science* **2000**, *287*, 1463−1466.

(19) Ruparelia, J. P.; Chatterjee, A. K.; Duttagupta, S. P.; Mukherji, S. Strain Specificity in Antimicrobial Activity of Silver and Copper Nanoparticles. *Acta. Biomater.* **2008**, *4*, 707−716.

(20) Rispoli, F.; Angelov, A.; Badia, D.; Kumar, A.; Seal, S.; Shahb, V. Understanding the Toxicity of Aggregated Zero Valent Copper Nanoparticles Against *Escherichia coli*. *J. Hazard. Mater.* **2010**, *180*, 212−216.

(21) Raffi, M.; Mehrwan, S.; Bhatti, T. M.; Akhter, J. I.; Hameed, A.; Yawar, W.; Hasan, M. M. Investigations into the Antibacterial Behavior of Copper Nanoparticles Against *Escherichia coli*. *Ann. Mcrobiol.* **2010**, *60*, 75−80.

(22) Kohlman, R. S.; Zibold, A.; Tanner, D. B.; Ihas, G. G.; Ishiguro, T.; Min, Y. G.; MacDiarmid, A. G.; Epstein, A. J. Limits for Metallic Conductivity in Conducting Polymers. *Phys. Rev. Lett.* **1997**, *78*, 3915−3918.

(23) Wu, C. S. Aliphatic-Aromatic Polyester-Polyaniline Composites: Preparation, Characterization, Antibacterial Activity, and Conducting Properties. *Polym. Int.* **2012**, *61*, 1556−1563.

(24) Sharma, S.; Nirkhe, C.; Pethkar, S.; Athawale, A. A. Chloroform Vapour Sensor Based on Copper/Polyaniline Nanocomposite. *Sens. Actuators, B* **2002**, *85*, 131−136.

(25) Seshadri, D. T.; Bhat, N. V. Use of Polyaniline as an Antimicrobial Agent in Textiles. *Indian J. Fibre Text. Res.* **2005**, *30*, 204−206.

(26) Shi, N.; Guo, X.; Jing, H.; Gong, J.; Sun, C.; Yang, K. Antibacterial Effect of the Conducting Polyaniline. *J. Mater. Sci. Technol.* **2006**, *22*, 289−290.

(27) Bogdanović, U.; Lazić, V.; Vodnik, V.; Budimir, M.; Marković, Z.; Dimitrijević, S. Copper Nanoparticles with High Antimicrobial Activity. *Mater. Lett.* **2014**, *128*, 75−78.

(28) Bogdanović, U.; Vodnik, V. V.; Ahrenkiel, S. P.; Stoiljković, M.; Ćirić-Marjanović, G.; Nedeljković, J. M. Interfacial Synthesis and Characterization of Gold/Polyaniline Nanocomposites. *Synth. Met.* **2014**, *195*, 122−131.

(29) Han, J.; Li, L.; Guo, R. Novel Approach to Controllable Synthesis of Gold Nanoparticles Supported on Polyaniline Nanofibers. *Macromolecules* **2010**, *43*, 10636−10644.

(30) Wang, X.; Wang, X.; Wu, Y.; Bao, L.; Wang, H. Interfacial Synthesis of Polyaniline Nanostructures Induced by 5-Sulfosalicylic Acid. *Mater. Lett.* **2010**, *64*, 1865−1867.

(31) Abdiryim, T.; Xiao-Gang, Z.; Jamal, R. Comparative Studies of Solid-State Synthesized Polyaniline Doped with Inorganic Acids. *Mater. Chem. Phys.* **2005**, *90*, 367−372.

(32) Li, X.; Bian, C.; Chen, W.; He, J.; Wang, Z.; Xu, N.; Xue, G. Polyaniline on Surface Modification of Diatomite: A Novel Way to Obtain Conducting Diatomite Fillers. *Appl. Surf. Sci.* **2003**, *207*, 378−383.

(33) Kim, B.-J.; Oh, S.-G.; Han, M.-G.; Im, S.-S. Synthesis and Characterization of Polyaniline Nanoparticles in SDS Micellar Solutions. *Synth. Met.* **2001**, *122*, 297−304.

(34) Han, M. G.; Cho, S. K.; Oh, S. G.; Im, S. S. Preparation and Characterization of Polyaniline Nanoparticles Synthesized from DBSA Miccelar Solution. *Synth. Met.* **2002**, *126*, 53−60.

(35) Kinyanjui, J. M.; Hatchett, D. W. Chemical Synthesis of a Polyaniline/Gold Composite Using Tetrachloroaurate. *Chem. Mater.* **2004**, *16*, 3390−3398.

(36) Venugopal, G.; Quan, X.; Johnson, G. E.; Houlihan, F. M.; Chin, E.; Nalamasu, O. Photoinduced Doping and Photolithography of Methyl-Substituted Polyaniline. *Chem. Mater.* **1995**, *7*, 271−276.

(37) Vossmeyer, T.; Katsikas, L.; Giersig, M.; Popovic, I. G.; Diesner, K.; Chemseddine, A.; Eychmueller, A.; Weller, H. CdS Nanoclusters: Synthesis, Characterization, Size Dependent Oscillator Strength, Temperature Shift of the Excitonic Transition Energy, and Reversible Absorbance Shift. *J. Phys. Chem.* **1994**, *98*, 7665−7673.

(38) Zhang, H.; Yu, X.; Braun, P. V. Three-Dimensional Bicontinuous Ultrafast-Charge and -Discharge Bulk Battery Electrodes. *Nat. Nanotechnol.* **2011**, *6*, 277−281.

(39) Khan, Z.; Al-Thabaiti, S. A.; Obaid, A. Y.; Al-Youbi, A. O. Preparation and Characterization of Silver Nanoparticles by Chemical Reduction Method. *Colloids Surf., B* **2011**, *82*, 513−517.

(40) Bober, P.; Trchova, M.; Prokeš, J.; Varga, M.; Stejskal, J. Polyaniline−Silver Composites Prepared by the Oxidation of Aniline with Silver Nitrate in Solutions of Sulfonic Acids. *Electrochim. Acta* **2011**, *56*, 3580−3585.

(41) Kitani, A.; Yano, J.; Sasaki, K. ECD Materials for the Three Primary Colors Developed by Polyanilines. *J. Electroanal. Chem.* **1986**, *209*, 227−232.

(42) Pouget, J. P.; Józefowicz, M. E.; Epstein, A. J.; Tang, X.; MacDiarmid, A. G. X-ray Structure of Polyaniline. *Macromolecules* **1991**, *24*, 779−789.

(43) Jozefowicz, M. E.; Laversanne, R.; Javadi, H. H. S.; Epstein, A. J. Multiple Lattice Phases and Polaron-Lattice-Spinless-Defect Competition in Polyaniline. *Phys. Rev. B* **1989**, *39*, 12958−12961.

(44) Rezaei, S. J. T.; Bide, Y.; Nabid, M. R. A New Approach for the Synthesis of Polyaniline Microstructures with a Unique Tetragonal Star-Like Morphology. *Synth. Met.* **2011**, *161*, 1414−1419.

(45) Zhang, L.; Wan, M. Self-Assembly of Polyaniline—From Nanotubes to Hollow Microspheres. *Adv. Funct. Mater.* **2003**, *13*, 815−820.

(46) Yu, Q.; Shi, M.; Cheng, Y.; Wang, M.; Chen, H. Z. Fe₃O₄@Au/Polyaniline Multifunctional Nanocomposites: Their Preparation and Optical, Electrical, and Magnetic Properties. *Nanotechnology* **2008**, *19*, 265702 (6 pp)..

(47) Hatchett, D. W.; Josowicz, M.; Janata, J. Acid Doping of Polyaniline: Spectroscopic and Electrochemical Studies. *J. Phys. Chem. B* **1999**, *103*, 10992−10998.

(48) Janošević, A.; Ćirić-Marjanović, G.; Marjanović, B.; Holler, P.; Trchová, M.; Stejskal, J. Synthesis and Characterization of Conducting Polyaniline 5-Sulfosalicylate Nanotubes. *Nanotechnology* **2008**, *19*, 135606−135613.

(49) Khan, M. M. R.; Wee, Y. K.; Mahmood, W. A. K. Effects of CuO on the Morphology and Conducting Properties of PANI Nanofibers. *Synth. Met.* **2012**, *162*, 1065−1072.

(50) Kang, E. T.; Neoh, K. G.; Tan, K. L. Polyaniline: A Polymer with many Interesting Intrinsic Redox States. *Prog. Polym. Sci.* **1998**, *23*, 277−324.

(51) Socrates, G. *Infrared and Raman Characteristic Group Frequencies: Tables and Charts*. Wiley: New York, 2001; pp 65−84, 107−109, 157−165, 249−261.

(52) Boomi, P.; Prabu, H. G.; Manisankar, P.; Ravikumarb, S. Study on Antibacterial Activity of Chemically Synthesized PANI-Ag-Au Nanocomposite. *Appl. Surf. Sci.* **2014**, *300*, 66−72.

(53) Thiel, J.; Pakstis, L.; Buzzby, S.; Raffi, M.; Ni, C.; Pochan, D. J.; Shah, I. Antibacterial Properties of Silver-Doped Titania. *Small* **2007**, *3*, 799−803.

(54) Madigan, M.; Martinko, J. *Brock Biology of Microorganisms*, 9th ed; Prentice-Hall: Upper Saddle River, NJ, 2005.

(55) Manzl, C.; Enrich, J.; Ebner, H.; Dallinger, R.; Krumschnabel, G. Copper-Induced Formation of Reactive Oxygen Species Causes Cell Death and Disruption of Calcium Homeostasis in Trout Hepatocytes. *Toxicology* **2004**, *196*, 57−64.

(56) Vollmer, W.; Blanot, D.; de Pedro, M. A. Peptidoglycan Structure and Architecture. *FEMS Microbiol. Rev.* **2008**, *32*, 149−167.

(57) Weidenmaier, C.; Peschel, A. Teichoic Acids and Related Cell-Wall Glycopolymers in Gram-Positive Physiology and Host Interactions. *Nat. Rev. Microbiol.* **2008**, *6*, 276−287.

(58) Beveridge, T. J.; Murray, R. G. E. Sites of Metal Deposition in the Cell Wall of *Bacillus subtilis*. *J. Bacteriol.* **1980**, *141*, 876−887.

(59) Fleet, G. In *Cell Walls*; Rose, A., Harrison, J., Eds.; Academic: London, 1991; pp 199.

(60) Lipke, P. N.; Ovalle, R. Cell Wall Architecture in Yeast: New Structure and New Challenges. *J. Bacteriol.* **1998**, *180*, 3735−3740.

(61) Milewski, A.; Andruszkiewicz, R.; Kasprzak, L.; Mazerski, J.; Mignini, F.; Borowski, E. Mechanism of Action of Anticandidial Dipeptides Containing Inhibitors of Glycocyamine-6-Phosphatase Synthase. *Antimic. Agent. Chem.* **1991**, *35*, 36−43.

(62) Linares, C. E. B.; Griebeler, D.; Cargnelutti, D.; Alves, S. H.; Morsch, V. M.; Schetinger, M. R. C. Catalase Activity in *Candida albicans* Exposed to Antineoplastic Drugs. *J. Med. Microbiol.* **2006**, *55*, 259−262.

(63) Hoshino, N.; Kimura, T.; Yamaji, A.; Ando, T. Damage to the Cytoplasmic Membrane of *Escherichia coli* by Catechin-Copper (II) Complexes. *Free Radical Biol. Med.* **1999**, *27*, 1245−1250.

(64) Ralph, A.; McArdle, H. J. Copper Metabolism and Requirements in the Pregnant Mother, Her Fetus, and Children. International Copper Association: New York, 2001.

(65) Zhang, Z.; Berg, A.; Levanon, H.; Fessenden, R. W.; Meisel, D. On the Interaction of Free Radicals with Gold Nanoparticles. *J. Am. Chem. Soc.* **2003**, *125*, 7959−7963.

(66) Yoon, K. Y.; Byeon, H. J.; Park, J. H.; Hwang, J. Susceptibility Constants of *Escherichia coli* and *Bacillus subtilis* to Silver and Copper Nanoparticles. *Sci. Total Environ.* **2007**, *373*, 572−575.

(67) Cioffi, N.; Ditaranto, N.; Torsi, L.; Picca, R. A.; Sabbatini, L.; Valentini, A.; Novello, L.; Tantillo, G.; Bleve-Zacheo, T.; Zambonin, P. G. Analytical Characterization of Bioactive Fluoropolymer Ultra-Thin Coatings Modified by Copper Nanoparticles. *Anal. Bioanal. Chem.* **2005**, *381*, 607−616.

(68) Morones, J. R.; Elechiguerra, J. L.; Camacho, A.; Holt, K.; Kouri, J.; Ramirez, J. T.; Yacaman, M. J. The Bactericidal Effect of Silver Nanoparticles. *Nanotechnology* **2005**, *16*, 2346−2353.

(69) Hatchett, D. W.; Henry, S. Electrochemistry of Sulfur Adlayers on the Low-Index Faces of Silver. *J. Phys. Chem.* **1996**, *100*, 9854−9859.